

PROCEEDINGS OF SPIE

Infrared Technology and Applications XLIII

Bjørn F. Andresen
Gabor F. Fulop
Charles M. Hanson
John L. Miller
Paul R. Norton
Editors

9–13 April 2017
Anaheim, California, United States

Sponsored and Published by
SPIE

Volume 10177

Proceedings of SPIE 0277-786X, V. 10177

SPIE is an international society advancing an interdisciplinary approach to the science and application of light.

Infrared Technology and Applications XLIII, edited by Bjørn F. Andresen, Gabor F. Fulop, Charles M. Hanson, John L. Miller, Paul R. Norton, Proc. of SPIE Vol. 10177, 1017701 · © 2017 SPIE
CCC code: 0277-786X/17/\$18 · doi: 10.1117/12.2280471

Proc. of SPIE Vol. 10177 1017701-1

The papers in this volume were part of the technical conference cited on the cover and title page. Papers were selected and subject to review by the editors and conference program committee. Some conference presentations may not be available for publication. Additional papers and presentation recordings may be available online in the SPIE Digital Library at SPIDigitalLibrary.org.

The papers reflect the work and thoughts of the authors and are published herein as submitted. The publisher is not responsible for the validity of the information or for any outcomes resulting from reliance thereon.

Please use the following format to cite material from these proceedings:

Author(s), "Title of Paper," in *Infrared Technology and Applications XLIII*, edited by Bjørn F. Andresen, Gabor F. Fulop, Charles M. Hanson, John L. Miller, Paul R. Norton, Proceedings of SPIE Vol. 10177 (SPIE, Bellingham, WA, 2017) Seven-digit Article CID Number.

ISSN: 0277-786X
ISSN: 1996-756X (electronic)

ISBN: 9781510608559
ISBN: 9781510608566 (electronic)

Published by

SPIE

P.O. Box 10, Bellingham, Washington 98227-0010 USA
Telephone +1 360 676 3290 (Pacific Time) · Fax +1 360 647 1445
SPIE.org

Copyright © 2017, Society of Photo-Optical Instrumentation Engineers.

Copying of material in this book for internal or personal use, or for the internal or personal use of specific clients, beyond the fair use provisions granted by the U.S. Copyright Law is authorized by SPIE subject to payment of copying fees. The Transactional Reporting Service base fee for this volume is \$18.00 per article (or portion thereof), which should be paid directly to the Copyright Clearance Center (CCC), 222 Rosewood Drive, Danvers, MA 01923. Payment may also be made electronically through CCC Online at copyright.com. Other copying for republication, resale, advertising or promotion, or any form of systematic or multiple reproduction of any material in this book is prohibited except with permission in writing from the publisher. The CCC fee code is 0277-786X/17/\$18.00.

Printed in the United States of America.

Publication of record for individual papers is online in the SPIE Digital Library.

SPIE. DIGITAL LIBRARY
SPIDigitalLibrary.org

Paper Numbering: *Proceedings of SPIE* follow an e-First publication model. A unique citation identifier (CID) number is assigned to each article at the time of publication. Utilization of CIDs allows articles to be fully citable as soon as they are published online, and connects the same identifier to all online and print versions of the publication. SPIE uses a seven-digit CID article numbering system structured as follows:

- The five digits correspond to the SPIE volume number.
- The last two digits indicate publication order within the volume using a Base 36 numbering system employing both numerals and letters. These two-number sets start with 00, 01, 02, 03, 04, 05, 06, 07, 08, 09, 0A, 0B ... 0Z, followed by 10-1Z, 20-2Z, etc. The CID Number appears on each page of the manuscript.

Contents

- ix *Authors*
- xiii *Conference Committee*
- xvii *Introduction*

NIR/SWIR I

- 10177 02 **Performance estimation for SWIR cameras under OH night airglow illumination** [10177-1]
- 10177 03 **Development of low-SWaP and low-noise InGaAs detectors** [10177-2]
- 10177 05 **Recent advances in InAs/InAs_{1-x}Sb_x/AlAs_{1-x}Sb_x gap-engineered type-II superlattice-based photodetectors (Invited Paper)** [10177-4]
- 10177 06 **Al/Sb free InGaAs unipolar barrier infrared detectors** [10177-5]
- 10177 07 **Low-noise readout circuit for SWIR focal plane arrays** [10177-6]
- 10177 08 **Progress on MCT SWIR modules for passive and active imaging applications** [10177-7]
- 10177 09 **Extended spectrum SWIR camera with user-accessible Dewar** [10177-8]

NIR/SWIR II

- 10177 0A **Numerical modeling of a dark current suppression mechanism in IR detector arrays** [10177-9]
- 10177 0B **Functionalization of graphene by size and doping control and its optoelectronic applications** [10177-10]
- 10177 0C **Military reconnaissance platform for the spectral range from the visible to the MWIR** [10177-11]

IR IN AIR AND SPACE

- 10177 0G **Recent progress of push-broom infrared hyper-spectral imager in SITP (Invited Paper)** [10177-14]
- 10177 0H **Infrared hyperspectral imaging miniaturized for UAV applications (Invited Paper)** [10177-15]
- 10177 0J **MWIR hyperspectral imaging with the MIDAS instrument (Invited Paper)** [10177-17]

10177 OK **CubeSat infrared atmospheric sounder (CIRAS) NASA InVEST technology demonstration (Invited Paper)** [10177-18]

10177 OL **Turret indirect vision systems (TIVS) replacing episcopes on armored fighting vehicles** [10177-102]

T2SL: VISTA I

10177 ON **Antimonide type-II superlattice barrier infrared detectors (Invited Paper)** [10177-22]

10177 OT **Advances in III-V based dual-band MWIR/LWIR FPAs at HRL (Invited Paper)** [10177-28]

10177 OU **Advances in III-V bulk and superlattice-based high operating temperature MWIR detector technology (Invited Paper)** [10177-29]

T2SL: NON-VISTA

10177 11 **Photodetector development at Fraunhofer IAF: From LWIR to SWIR operating from cryogenic close to room temperature** [10177-36]

10177 12 **Growth and characterization of $\text{In}_{1-x}\text{Ga}_x\text{As}/\text{InAs}_{0.65}\text{Sb}_{0.35}$ strained layer superlattice infrared detectors** [10177-37]

10177 13 **T2SL production and development at IRnova: From MWIR to VLWIR detection** [10177-38]

10177 14 **Development of Type-II superlattice VLWIR detectors in JAXA** [10177-40]

10177 15 **InAs/GaSb type-II superlattice infrared detectors: three decades of development** [10177-99]

KEYNOTE SESSION

10177 16 **The development of the infrared technology for meteorological satellites in Shanghai Institute of Technical Physics (Keynote Paper)** [10177-41]

SUBSTRATES

10177 17 **Bulk growth and surface characterization of epitaxy ready cadmium zinc telluride substrates for use in IR imaging applications** [10177-42]

10177 18 **Large-format multi-wafer production of 5" GaSb-based photodetectors by molecular beam epitaxy** [10177-43]

HGCDTE

- 10177 19 **Response time improvement of LWIR HOT MCT detectors** [10177-44]
- 10177 1A **Ultra-compact high-performance MCT MWIR engine** [10177-45]
- 10177 1B **Simulation of infrared avalanche photodiodes from first principles** [10177-46]
- 10177 1C **Microstructure characterization of lattice defects induced by As ion implantation in HgCdTe epilayers** [10177-47]
- 10177 1D **General review of multispectral cooled IR development at CEA-Leti, France** [10177-48]
- 10177 1E **Latest improvements on long wave p on n HgCdTe technology at Sofradir** [10177-49]
- 10177 1G **Daphnis 10 μ m pixel pitch product: optimized product and process postponements allowing outstanding on-time delivery** [10177-51]
- 10177 1H **A comparative design study for MWIR HgCdTe detectors** [10177-52]

HOT I

- 10177 1I **10 μ m pitch family of InSb and X_{Bn} detectors for MWIR imaging** [10177-53]
- 10177 1J **Fabrication of small pitch, high definition (HD) 1kx2k/5 μ m MWIR focal-plane-arrays operating at high temperature (HOT)** [10177-54]
- 10177 1K **State-of-the-art MCT photodiodes for cutting-edge sensor applications by AIM** [10177-55]
- 10177 1L **MWIR barrier infrared detectors with greater than 5 μ m cutoff using bulk InAsSb grown on GaSb substrates** [10177-56]
- 10177 1M **High quantum efficiency mid-wavelength infrared superlattice photodetector** [10177-59]

HOT II

- 10177 1O **Heterojunction phototransistor for highly sensitive infrared detection** [10177-60]
- 10177 1P **Evidence of carrier localization in InAsSb/InSb digital alloy nBn detector** [10177-61]
- 10177 1Q **Effects of epitaxial structure and processing on electrical characteristics of InAs-based nBn infrared detectors** [10177-62]

UNCOOLED FPAS AND APPLICATIONS

- 10177 1R **Novel vacuum packaged 384x288 broadband bolometer FPA with enhanced absorption in the 3-14 μ m wavelength range** [10177-63]

- 10177 1S **High-performance mushroom plasmonic metamaterial absorbers for infrared polarimetric imaging** [10177-64]
- 10177 1T **Uncooled infrared photodetectors based on one-dimensional nanowires and two-dimensional materials (Invited Paper)** [10177-65]
- 10177 1U **A low-power CMOS readout IC design for bolometer applications** [10177-66]
- 10177 1W **Spectral response of microbolometers for hyperspectral imaging** [10177-69]
- 10177 1X **An 80x80 microbolometer type thermal imaging sensor using the LWIR-band CMOS infrared (CIR) technology** [10177-100]
- 10177 1Y **An advanced presence detection system using the CMOS Infrared (CIR) technology** [10177-101]

ROIC

- 10177 1Z **A PFM-based MWIR DROIC employing off-pixel fine conversion of photocharge to digital using integrated column ADCs** [10177-70]
- 10177 20 **Development of a fully programmable ROIC with 15 μm pixel pitch for MWIR applications** [10177-71]

SMART PROCESSING

- 10177 25 **Small pixel infrared sensor technology (Invited Paper)** [10177-78]

A WORD FROM THE MASTERS

- 10177 26 **Infrared engineering for the advancement of science: A UK perspective (Invited Paper)** [10177-79]
- 10177 27 **My life in IRFPA Research and Development (Invited Paper)** [10177-80]

QWIP AND Q-DOTS

- 10177 29 **Effects of doping on photoelectron kinetics and characteristics of quantum dot infrared photodetector** [10177-82]
- 10177 2A **Resonator-QWIPs for 10.6 micron detection** [10177-83]
- 10177 2B **Towards flexible quantum well infrared photodetectors** [10177-84]
- 10177 2C **Novel high-resolution VGA QWIP detector** [10177-85]

POSTER SESSION

- 10177 2D **Minority carrier diffusion lengths and mobilities in low-doped n-InGaAs for focal plane array applications** [10177-86]
- 10177 2E **Effect of insulator layer in graphene plasmonic metamaterials for infrared detection** [10177-87]
- 10177 2G **Remote pedestrians detection at night time in FIR Image using contrast filtering and locally projected region based CNN** [10177-89]
- 10177 2H **A study on inductively coupled plasma etch rate of HgCdTe at cryogenic temperature** [10177-90]
- 10177 2I **Forward looking infrared imagery for landmine detection** [10177-91]
- 10177 2J **Design and fabrication of metal-insulator-metal diode for high frequency applications** [10177-92]
- 10177 2K **Array size and area impact on nanorectenna performance properties** [10177-94]
- 10177 2L **Standardizing large format 5" GaSb and InSb substrate production** [10177-95]
- 10177 2M **Short wavelength infrared photodetector and light emitting diode based on InGaAsSb** [10177-96]

Authors

Numbers in the index correspond to the last two digits of the seven-digit citation identifier (CID) article numbering system used in Proceedings of SPIE. The first five digits reflect the volume number. Base 36 numbering is employed for the last two digits and indicates the order of articles within the volume. Numbers start with 00, 01, 02, 03, 04, 05, 06, 07, 08, 09, 0A, 0B...0Z, followed by 10-1Z, 20-2Z, etc.

Abbasi, Shahbaz, 1U, 1Z
Adelmini, L., 1D
Akar, Orhan Sevket, 1X
Akbulut, Mehmet, 07, 20
Akin, Tayfun, 1X, 1Y
Akyurek, Fatih, 07, 20
Alain, Christine, 1R
Altun, Oguz, 07, 20
Alverbro, J., 2C
Aravazhi, Shanmugam, 2L
Ariyawansa, Gamini, 12, 1M
Aron, Yoram, 0L
Arslan, Tugay, 1Y
Arsoy, Elif Gul, 1U, 2K
Askar, Hidir, 1X
Asplund, C., 13, 2C
Avnon, E., 1I
Azad, Ibrahim, 2J
Badano, G., 1D
Baker, Ian M., 26
Ballet, P., 1D
Bandara, Sumith, 1L
Baril, Neil, 1L
Baudry, X., 1D
Baylet, J., 1D
Bayram, Aylin, 2I
Beaupré, Patrick, 1R
Becanovic, S., 2C
Beetz, J., 1K
Béland, David, 1R
Bellotti, Enrico, 0A
Benapfl, Brendan, 09
Benecke, M., 08
Berkowicz, E., 03
Berthoz, Jocelyn, 1E
Betz, T. E. M., 17
Bikov, L., 03
Bisotto, S., 1D
Bornfreund, R. E., 2A
Boulard, F., 1D
Bozdağı Akar, Gözde, 2I
Breiter, R., 08, 1A, 1K
Brown, Alexander, 1L
Brudevoll, Trond, 1B
Brumer, M., 1I
Brunner, Alexandre, 1E
Burgess, L., 17
Castelein, P., 1D
Caulfield, John, 0U, 1J, 25
Ceylan, Ömer, 1U, 1Z
Chen, J. X., 16
Chen, Lu, 1C
Chen, Xiaoshuang, 16, 1T
Chen, Y. Y., 2H
Chevallier, Romain, 05
Choi, K. K., 2A
Cilbir, Gorkem, 1Y
Cologlu, Mustafa H., 1X
Compain, Valery, 1G
Costard, E., 13, 2C
Cowan, Vincent M., 1M
Curzan, J. P., 0U, 1J, 25
Dallas, G., 2L
Dargent, L., 1E
Daumer, V., 1I
De Lyon, T. J., 0U, 1J
De Monte, Bertrand, 1G
DeCuir, E. A., 2A
Dehzangi, Arash, 05
Delaunay, Pierre-Yves, 0T
Denhoff, Mike W., 2D
Deshaies, Sébastien, 1R
Ding, L., 16
Ding, R. J., 2H
Du, X., 1Q
Dufour, Denis, 1R
Dumanli, Hilal K., 1X
Duran, J. M., 12
Durmaz, Emre Can, 1U, 2K
Eich, D., 08, 1A, 1K
Elishkov, R., 03
Espiau de Lamaestre, R., 1D
Evans, D., 2C
Fang, Hehai, 1T
Fastenau, Joel M., 18, 1L
Figgemeier, H., 08, 1A, 1K
Fisette, Bruno, 1R
Fisher, Anita M., 0N, 1P
Flint, J. Patrick, 17, 2L
Fraenkel, R., 03
Freiman, W., 1I
Frey, Phillip, 18
Fries, P., 1K
Fritze, J., 0C
Fujisawa, Daisuke, 1S, 2E
Furlong, Mark J., 18, 2L
Galioglu, Arman, 1U, 1Z
Gamfeldt, A., 13
Garduno, Eli, 1M
Gawron, W., 19

Gay, David, 1R
 Génèreux, Francis, 1R
 Gerken, M., 0C
 Gershon, G., 1I
 Giladi, A., 03
 Glasmann, Andreu, 0A
 Goldar, Dara, 1B
 Goswami, D. Yogi, 2J
 Gramich, V., 1I
 Grangier, C., 1D
 Gravrand, O., 1D
 Grein, Christoph, 09
 Guinedor, Pierre, 1E
 Gunapala, Sarath D., 0N, 1P
 Gurbuz, Yasar, 1U, 1Z, 2K
 Gurga, Alexander R., 0T
 Haddadi, Abbas, 05
 Hanna, S., 1K
 Hata, Hisatoshi, 1S
 He, L., 16, 2H
 Hill, Cory J., 0N, 1P
 Hinnrichs, Bradford, 0H
 Hinnrichs, Michele, 0H
 Hiroe, Yuta, 14
 Hirsh, I., 03
 Höglund, Linda, 0N, 13, 2C
 Honniball, Casey I., 0J, 1W
 Hu, Weida, 0G, 1T
 Hubbard, Taylor, 0A
 Iguchi, Yasuhiro, 02, 14
 Ilan, E., 03
 Inada, Hiroshi, 02, 14
 Inceturkmen, Ercihan, 07, 20
 Jakobson, C., 03
 Jenkins, J., 0U, 1J
 Ji, Rongbin, 0B
 Julien, Christian, 1R
 Kagami, Sota, 02
 Kang, Sang-Woo, 2M
 Karaca, Utku, 06
 Karni, Y., 1I
 Kataria, H., 13, 2C
 Katsuyama, Tsukuru, 02
 Kattner, Michael, 18
 Kaynak, Mehmet, 1U
 Kazemi, Alireza, 1M
 Kębtowski, A., 19
 Keo, Sam A., 0N, 1P
 Kepenek, Reha, 07, 20
 Kerlain, A., 1E
 Khoshakhlagh, Arezou, 0N, 1P
 Kim, Jun Oh, 2M
 Kim, Sungcho, 2G
 Kim, Taehwan, 2G
 Kimata, Masafumi, 14, 1S, 27
 Kimura, Toshiyoshi, 14
 Kizilkan, Ekin, 06
 Kocaman, Serdar, 06, 1H
 Kondrashov, P., 03
 Kong, Jincheng, 0B
 Kopytko, M., 15, 19
 Krishna, Sanjay, 1M
 Ku, Zahyun, 2M
 Kuboyama, Takafumi, 1S
 Kumar, F. J., 17
 Kumeta, Ayaka, 14
 Lee, Sang Jun, 2M
 Lee, Seung Hyun, 1M
 Li, Chunlai, 0G
 Li, Shilong, 2B
 Li, X. Y., 16
 Lin, Chun, 1C
 Lindberg, A., 2C
 Liu, Amy W. K., 18, 1L
 Liu, F. L., 2H
 Liu, John K., 0N
 Loubychev, Dmitri, 18, 1L
 Louzon, E., 03
 Lu, Wei, 16, 1T, 2B
 Lucey, Paul G., 0J, 1W
 Luo, Wenjin, 1T
 Luong, Edward M., 0N
 Lutz, H., 1A
 Mackenzie, J., 17
 Madejczyk, P., 19
 Mahlein, K.-M., 1K
 Maillard, Magalie, 1E
 Manissadjian, A., 1E
 Marcks von Würtemberg, R., 13
 Marmonier, F., 1D
 Marozas, B. T., 1Q
 Martinez, Becky, 17, 2L
 Martyniuk, P., 15, 19
 Mathews, Sen, 1M
 Matsumoto, Kazuhiko, 2E
 Mazaleyrat, Eric, 1G
 McCutchen, Earl, 0H
 Mei, Yongfeng, 2B
 Miller, John Lester, 09
 Mitin, Vladimir, 29
 Mohseni, Hooman, 1O
 Morath, Christian, 1M
 Müller, R., 1I
 Mumolo, Jason M., 0N
 Münzberg, M., 0C
 Murooka, Jumpei, 14
 Myers, Stephen, 1M
 Nambu, Yoshihiro, 02
 Nevo, I., 03
 Nguyen, Jean, 0N
 Nguyen, Tien Dai, 2M
 Niderman, T., 1I
 Noshu, Brett Z., 0T
 Nuzumlali, Omer Lutfi, 07, 20
 Oda, Naoki, 02
 Oelmaier, R., 1A
 Ofer, O., 1I
 Ogawa, Shinpei, 1S, 2E
 Oktyabrsky, Serge, 29
 Orlach, Bertrand, 1G
 Oruc, Feyza, 1X
 Oulachgar, Hassane, 1R

Ozcan, Meric, 2K
 Ozer, Yigit, 1H
 Ozturk, Hande, 1X
 Pagano, Thomas S., 0K
 Panzarella, Florent, 1G
 Park, Min-Su, 1O
 Pepper, Brian J., 0N, 1P
 Péré-Laperne, Nicolas, 1E
 Piotrowski, A., 19
 Piotrowski, J., 19
 Pivnik, I., 03
 Pusz, W., 19
 Rabinowitz, Cobi, 1O
 Rafol, Sir B., 0N
 Rajavel, Rajesh D., 0T, 0U, 1J
 Ram, Manoj K., 2J
 Razeghi, Manijeh, 05
 Rehm, R., 11
 Reibel, Y., 1E
 Reyner, C. J., 12
 Rezaei, Mohsen, 1O
 Roebuck, M., 0U, 1J
 Rogalski, A., 15, 19
 Rosenstock, T., 11
 Royer, Yves, 1G
 Rubaldo, Laurent, 1E
 Rutkowski, J., 19
 Rutz, F., 11
 Rutzinger, S., 1A
 Sablon, Kimberly, 29
 Sakai, Michito, 14
 Sano, Masahiko, 02
 Savich, G. R., 1Q
 Scheihing, John E., 12, 1M
 Schenk, H., 1A
 Schirmacher, W., 1K
 Schmidt, J., 11
 Schuler-Sandy, Ted, 1M
 Sehlin, S., 2C
 Seref, D., 11
 Sergeev, Andrei, 29
 Shafique, Atia, 1U, 1Z, 2K
 Sharifi, H., 0U, 1J
 Shi, Changzhi, 1C
 Shiloah, N., 11
 Shimatani, Masaaki, 2E
 Shkedy, L., 11
 Shtrichman, I., 11
 Shu, Rong, 0G
 Sieck, A., 08
 Sivananthan, Siva, 09
 Sjöström, F., 2C
 Smith, B., 2L
 Smuk, S., 2C
 Soibel, Alexander, 0N, 1P
 Stadelmann, T., 11
 Steenberg, Elizabeth H., 12, 1M
 Stefanakos, Elias, 2J
 Stępień, D., 19
 Storebø, Asta Katrine, 1B
 Strong, W., 0U, 1J
 Sun, J. G., 2A
 Taalat, Rachid, 1E
 Taghipour, Zahra, 1M
 Tan, Chee Leong, 1O
 Tanaka, Tomo, 02
 Tang, Libin, 0B
 Tankut, Firat, 1X
 Tasdemir, Ferhat, 07, 20
 Tepegoz, Murat, 1X, 1Y
 Terroux, Marc, 1R
 Terterian, Sevag, 0T, 0U, 1J
 Tessler, R., 11
 Tian, Pin, 0B
 Tidrow, Meimei, 1L
 Tilkioglu, Bilge, 1X
 Ting, David Z., 0N, 1P
 Tinghag, P., 2C
 Tokranov, Vadim, 29
 Tremblay, Bruno, 1R
 Tremblay, Mathieu, 1R
 Tu, B., 0U, 1J
 Tuito, A., 03
 Tunca, Can, 07, 20
 Tybjerg, M., 2L
 Uetsuki, Mitsuharu, 1S
 Ugur, Beril, 1X
 Urbas, Augustine, 2M
 Uzgur, Fatih, 06
 Varghese, Alex, 29
 Vasserman, S., 03
 Vemuri, Hari, 09
 Veyrier, Jacques, 1G
 Vivier, Stéphane, 1G
 Vollard, Gregory, 1G
 Walker, Alexandre W., 2D
 Wang, Han, 2B
 Wang, Jianyu, 0G
 Wang, Peng, 1T
 Wang, Yueming, 0G, 1T
 Wasserman, D., 12
 Weber, A., 08
 Wei, Yanfeng, 1C
 Weispfenning, M., 0C
 Wendler, J., 08, 1A
 Wenisch, J., 1K
 Wheaton, Skyler, 1O
 Wicks, G. W., 1Q
 Wörl, A., 11
 Wright, Rob, 0J, 1W
 Xiang, Jinzhong, 0B
 Yakimov, Michael, 29
 Yamamoto, Tsuyoshi, 02
 Yang, Thomas, 05
 Yazici, Melik, 1U, 1Z
 Ye, Z. H., 2H
 Yoon, N., 12
 Yuan, Liyin, 0G
 Zhang, Xiang, 29
 Zhen, Honglou, 2B
 Zuo, Daniel, 1L

Conference Committee

Symposium Chairs

Donald A. Reago Jr., U.S. Army Night Vision & Electronic Sensors Directorate (United States)

Arthur A. Morrish, Raytheon Space and Airborne Systems (United States)

Conference Chairs

Bjørn F. Andresen, RICOR-Cryogenic & Vacuum Systems (Israel)

Gabor F. Fulop, Maxtech International, Inc. (United States) and Infrared Imaging News (United States)

Charles M. Hanson, SenselR Solutions, LLC (United States)

John L. Miller, Cascade Electro Optics and Episensors (United States)

Paul R. Norton, U.S. Army Night Vision & Electronic Sensors Directorate (United States)

Conference Program Committee

Tayfun Akin, Mikro-Tasarim Ltd. (Turkey) and Middle East Technical University (Turkey)

Stefan T. Baur, Raytheon Vision Systems (United States)

Eric Belhaire, Thales Optronique S.A.S. (France)

Wolfgang A. Cabanski, AIM INFRAROT-MODULE GmbH (Germany)

John T. Caulfield, Cyan Systems (United States)

Eric Costard, IRnova AB (Sweden)

Ronald G. Driggers, St. Johns Optical Systems (United States)

Michael T. Eismann, Air Force Research Laboratory (United States)

Martin H. Effenberg, Princeton Infrared Technologies, Inc. (United States)

Mark E. Greiner, L-3 Communications Cincinnati Electronics (United States)

Sarath D. Gunapala, Jet Propulsion Laboratory (United States)

Weida Hu, Shanghai Institute of Technical Physics (China)

Masafumi Kimata, Ritsumeikan University (Japan)

Hee Chul Lee, KAIST (Korea, Republic of)

Paul D. LeVan, Air Force Research Laboratory (United States)

Jay S. Lewis, DARPA/MTO (United States)

Kevin C. Liddiard, Electro-optic Sensor Design (Australia)

Wei Lu, Shanghai Institute of Technical Physics (China)

Tara J. Martin, UTC Aerospace Systems (United States)

Whitney Mason, U.S. Army Night Vision & Electronic Sensors
Directorate (United States)

Paul L. McCarley, Air Force Research Laboratory (United States)

R. Kennedy McEwen, SELEX ES (United Kingdom)

A. Fenner Milton, U.S. Army Night Vision & Electronic Sensors
Directorate (United States)

Mario O. Münzberg, Airbus Defence and Space (Germany)

Peter W. Norton, BAE Systems (United States)

Vladimir P. Ponomarenko, Orion Research-and-Production
Association (Russian Federation)

Manijeh Razeghi, Northwestern University (United States)

Donald A. Reago Jr., U.S. Army Night Vision & Electronic Sensors
Directorate (United States)

Colin E. Reese, U.S. Army Night Vision & Electronic Sensors Directorate
(United States)

Patrick Robert, ULIS (France)

Antoni Rogalski, Military University of Technology (Poland)

Thomas R. Schimert, DRS Technologies, Inc. (United States)

Itay Shtrichman, SCD Semiconductor Devices (Israel)

Torbjørn Skauli, Norwegian Defence Research Establishment
(Norway)

Bharadwaja Srowthi, L-3 Communications Infrared Products
(United States)

Stefan P. Svensson, U.S. Army Research Laboratory (United States)

J. Ralph Teague, Georgia Tech Research Institute (United States)

William A. Terre, FLIR Systems, Inc. (United States)

Simon Thibault, University Laval (Canada)

Meimei Tidrow, U.S. Army Night Vision & Electronic Sensors Directorate
(United States)

Michel Vuillermet, SOFRADIR (France)

James R. Waterman, U.S. Naval Research Laboratory (United States)

Ami Yaacobi, Rafael Advanced Defense Systems Ltd. (Israel)

Lucy Zheng, Institute for Defense Analyses (United States)

Session Chairs

NIR/SWIR I

Mario O. Münzberg, Airbus Defence and Space (Germany)

NIR/SWIR II

Martin H. Ettenberg, Princeton Infrared Technologies, Inc.
(United States)

IR in Air and Space

Weida Hu, Shanghai Institute of Technical Physics of the Chinese
Academy of Sciences (China)

Sarath D. Gunapala, Jet Propulsion Laboratory (United States)

T2SL: VISTA I

Donald A. Reago Jr., U.S. Army Night Vision & Electronic Sensors
Directorate (United States)

Meimei Z. Tidrow, U.S. Army Night Vision & Electronic Sensors
Directorate (United States)

T2SL: VISTA II

Donald A. Reago Jr., U.S. Army Night Vision & Electronic Sensors
Directorate (United States)

Meimei Z. Tidrow, U.S. Army Night Vision & Electronic Sensors
Directorate (United States)

T2SL: Non-VISTA

Lucy Zheng, Institute for Defense Analyses (United States)

Meimei Z. Tidrow, U.S. Army Night Vision & Electronic Sensors
Directorate (United States)

Substrates

Lucy Zheng, Institute for Defense Analyses (United States)

Meimei Z. Tidrow, U.S. Army Night Vision & Electronic Sensors
Directorate (United States)

HgCdTe

Wei Lu, Shanghai Institute of Technical Physics of the Chinese
Academy of Sciences (China)

Ian Baker, Leonardo MW Ltd. (United Kingdom)

HOT I

Michael T. Eismann, Air Force Research Laboratory (United States)

Antoni Rogalski, Military University of Technology (Poland)

HOT II

Antoni Rogalski, Military University of Technology (Poland)

Michael T. Eismann, Air Force Research Laboratory (United States)

Uncooled FPAs and Applications

Kevin C. Liddiard, Electro-optic Sensor Design (Australia)

Colin E. Reese, U.S. Army Night Vision & Electronic Sensors Directorate
(United States)

Masafumi Kimata, Ritsumeikan University (Japan)

ROIC

John L. Miller, Cascade Electro Optics and Episensors
(United States)

John T. Caulfield, Cyan Systems (United States)

Smart Processing

John T. Caulfield, Cyan Systems (United States)

Paul L. McCarley, Air Force Research Laboratory (United States)

A Word from the Masters

Paul R. Norton, U.S. Army Night Vision & Electronic Sensors Directorate
(United States)

QWIP and Q-Dots

Eric M. Costard, IRnova AB (Sweden)

Introduction

The Forty-Second conference on Infrared Technology and Applications was held the week of April 9-13, 2017 at the Anaheim Convention Center in Anaheim, California. The agenda was divided into 16 sessions:

1. NIR/SWIR I
2. NIR/SWIR II
3. Infrared in Air and Space
4. Type II Superlattices VISTA I
5. Type II Superlattices VISTA II
6. Type II Superlattices Non-VISTA
7. Keynote Session
8. Substrates
9. HgCdTe
10. HOT I
11. HOT II
12. Uncooled FPAs and Applications
13. ROICs
14. Smart Processing
15. A Word from the Masters
16. QWIP and QDots

Note that two new conferences have been initiated to cover the topics of optics (Advanced Optics for Defense Applications: UV through LWIR) and coolers (Tri-Technology Device Refrigeration) that were previously part of this conference.

In addition, there were a number of poster papers presented for discussion on Tuesday evening—these have been added to the 15 sessions in the Proceedings. Highlights of five topical areas are summarized below:

- Photon Detectors
- Uncooled Detectors
- Smart Processing
- Applications
- Keynote Address

Photon Detectors

NIR/SWIR FPAs and Applications

InGaAs/InP continues to be the preferred detector type for SWIR operation up to a cutoff of $1.7 \mu\text{m}$. These FPAs are now available commercially in formats up to 1280×1024 with $10 \mu\text{m}$ pixels.

For extended SWIR (eSWIR)—with cutoffs to $2.5 \mu\text{m}$ and beyond—both MCT and Type II Superlattice (T2SL) detectors are being rapidly developed.

InGaAs

One company is improving the performance of its 640×512 InGaAs FPAs with $15 \mu\text{m}$ pixels so that they can compete with Image Intensified Night Vision. The dark current has been reduced to below 2 fA at 20°C in order to save TEC cooling power and a new ROIC having 15-electron readout noise has been designed.

In initial tests under starlight conditions, the FPA is said to perform significantly better than Gen II image intensifiers and comparable to Gen III image intensifiers. An image of two people at a distance of 100 m—under starlight conditions—is shown in Fig. 1.

HgCdTe

One company is using LPE-grown MCT to fabricate 640×512 , $10 \mu\text{m}$ pixel eSWIR FPAs with a cutoff of



Fig. 1 InGaAs image under starlight conditions.



Fig. 2 Comparison of eSWIR, SWIR, MWIR 640 x 512/15 MCT FPAs with I².

2.5 μm to allow a combination of reflective and emissive imaging by also detecting thermal radiation in the eSWIR band.

A comparison of eSWIR, SWIR, MWIR 640 x 512/15 MCT FPAs with an image intensified image under overcast light conditions is shown in Figure 2.

For production, the company expects to use MBE grown MCT on GaAs substrates. A clip-on weapon sight weighing 1.1 kg is being designed with this FPA.

Another company has designed a series of eSWIR cameras based on $\text{Hg}_{1-x}\text{Cd}_x\text{Te}$ absorbers. The cameras have a bandpass extending to 3 μm cutoff wavelength, and thus open up new applications beyond those available with traditional InGaAs-based cameras. The cameras also have user-accessible dewars that can be opened and modified in a standard laboratory environment, thus allowing for swapping of internal components such as cold filters and cold stops.

InGaAs/GaAsSb T2SL FPAs with a format of 320 x 256 have been developed and the cutoff has been extended to 2.5 μm . The longer cutoff is advantageous due to the amount of night air glow illumination that exists beyond the 1.7 μm cutoff of ordinary InGaAs.

One company calculated signal-to-noise ratios and contrasts for a T2SL SWIR camera (2.3 μm cutoff) and an InGaAs camera (cutoff 1.7 μm) in a situation

in which human skin, clothes and surrounding materials are illuminated only by night airglow and are observed with the SWIR cameras from a distance of 300 m.

The results indicated that (1) the signal-to-noise ratio for the T2SL camera is larger than that for the InGaAs camera, (2) the contrasts of human skin vs surroundings are positive for the T2SL camera, while those for the InGaAs camera are negative, and (3) the operating temperature of the T2SL FPA should be lower than that of the InGaAs FPA.

Researchers at Northwestern University have developed a Ga-free T2SL SWIR detector based on $\text{InAs}_{1-x}\text{Sb}_x/\text{AlAs}_{1-x}\text{Sb}_x$. At 1.7 μm , the saturated dark current shot noise limited D^* was 5.66×10^{12} Jones.

Type II superlattice FPAs—VISTA

A full day was given to papers reviewing the large, multi-year VISTA program. An introduction and overview were given by Drs. Don Reago and Meimei Tidrow.

Papers were presented covering the growth of GaSb substrates with increasingly-large diameters up to 5 inches for fabricating a larger number of arrays per wafer processed, and for making larger array sizes in the future. MBE epitaxial growth of the Sb compounds and alloys involved in both type-2 superlattice and barrier detectors technologies was described from several vendors.

Device designs and FPA results were presented in following papers. Fig. 3 shows an image taken with a



Fig. 3 Image taking from an 11 μm cutoff T2SL barrier infrared detector FPA with 99.4 % operability in a 1280 x 720 format.

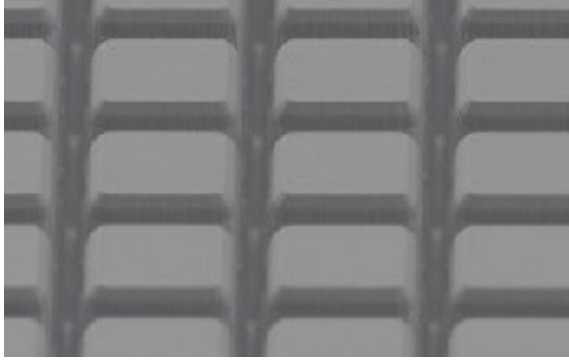


Fig. 4 Dry-etched SLS pixels with >76 % fill factor for 12 μm pitch.

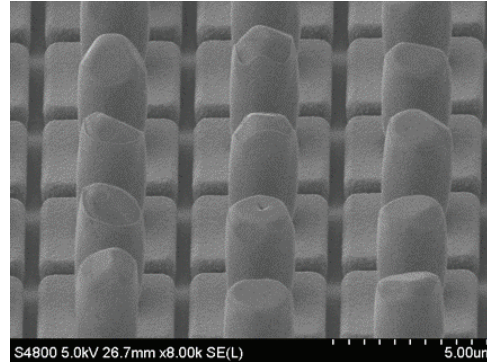


Fig. 6 An SEM photo of fabricated 5 μm pixels using a high-aspect ratio dry etch process resulting > 80% physical fill factor.

barrier detector design in an HD format array. Development of dry-etching technology enabled relatively high fill-factor for small, 12 μm pixels as shown in Fig. 4. Imagery from both bands of a dual-band MWIR/LWIR 1280 \times 720 format SLS array with 12 μm pixels produced by the VISTA program is shown in Fig. 5.

Small-pixel HOT arrays were also developed under the VISTA program. Fig. 6 shows 5 μm pixels from part of a large, 1 K \times 2 K array. The material is based on superlattice III-V absorbing layers grown by MBE on GaSb substrates. Using sub-frame averaging the NE ΔT was measured at <20 mK at 150 K.

All of the papers in sessions 4 and 5 were invited, presentation only. Three authors did submit papers nevertheless and these can be found in the proceedings.

Non-VISTA

Session 6 included Type II superlattice and barrier detectors from other programs. Reports of progress across the range from SWIR to LWIR were given. In one paper the I-V curves were shown for MWIR Type II devices with homo-junctions compared to hetero-junctions—see Fig. 7. Hetero-junctions had higher resistance. A SWIR FPA together with gated imagery was also discussed as illustrated in Fig. 8.

A wide variety of Type II designs were compared with respect to their absorption coefficient and other properties relevant to detector performance. The NE ΔT as a function of temperature for a promising design is illustrated in Fig. 9.

MWIR and LWIR Type II detector development was among the topics covered in another report. Improvements in quantum efficiency were achieved and the



Fig. 5 MWIR and LWIR images acquired with a 1280 \times 720 format SLS array with 12 μm pixels dual band MW/LW FPA fabricated on VISTA. The image was captured at 80 K and f/4.

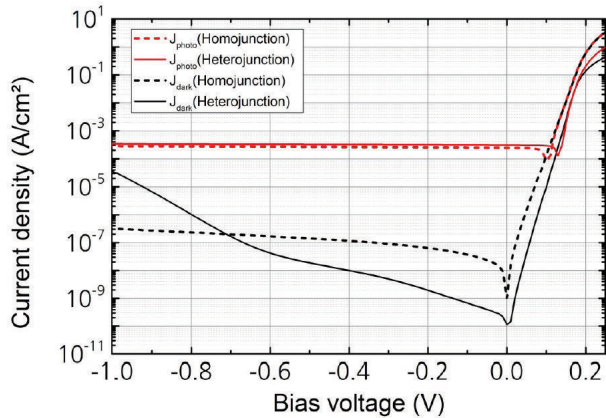


Fig. 7 Dark current (black) and photo current (red) density of a homojunction T2SL diode (dashed) and heterojunction diode (solid) with a comparable cut-off wavelength around $5 \mu\text{m}$ measured at 77 K.

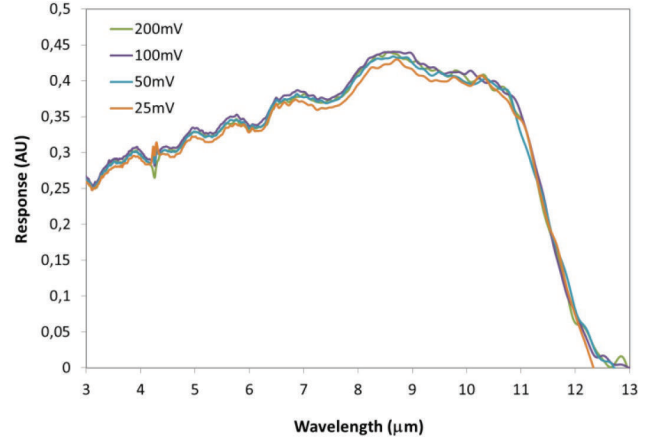


Fig. 10 Spectral response of an LWIR Type II detector having an $\sim 11.5 \mu\text{m}$ cutoff .



Fig. 8 Color-coded overlay of the distance dependent recording of a building with the SWIR gated viewing system.

spectral response of an LWIR detector with a cutoff of $11.5 \mu\text{m}$ was present—see Fig. 10.

A multi-year VLWIR— $15 \mu\text{m}$ cutoff—Type II detector development program is being carried out with the application in mind for FTIR instruments that measure the atmosphere's vertical temperature and water-vapor profile.

Substrates

This session reported on large diameter substrate development in support of both HgCdTe and Sb-based detector materials. CdZnTe boules were grown using the traveling heater method. GaSb boules are now being grown in sizes up to 5 inches. The progression of GaSb wafer size is shown in Fig. 11.

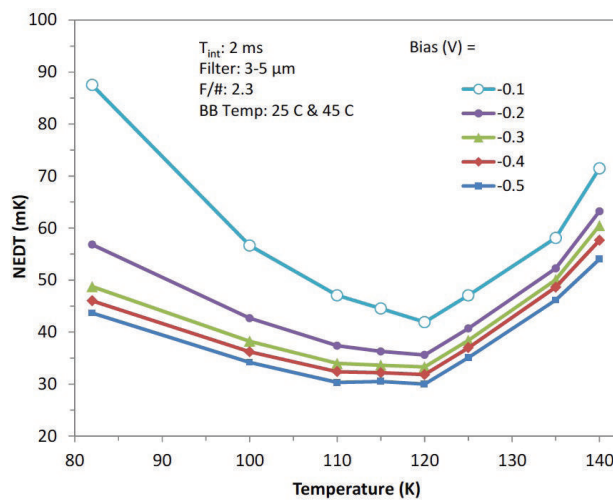


Fig. 9 Variation of median $NE\Delta T$ with temperature and bias at 2 ms integration time for an MWIR Type II detector design.

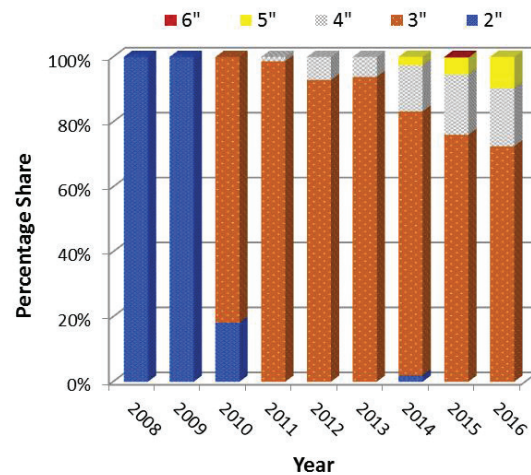


Fig. 11 Progression of GaSb epiwafer diameter.

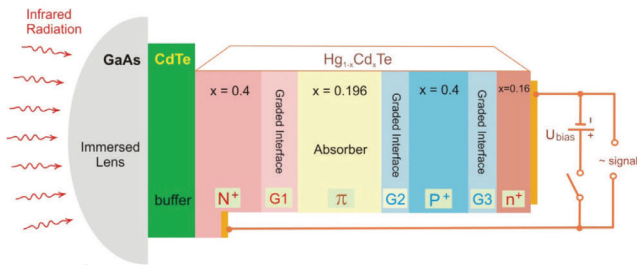


Fig. 12 The general design of an LWIR HgCdTe detector with graded interfaces.

HgCdTe

Mercury cadmium telluride technology continues to improve in a variety of ways to serve the wide variety of applications that depend upon this material. The first paper in this session discussed improving the response time of TE-cooled LWIR detectors that are important for spectroscopy and laser warning applications. The response time of these detectors revealed complex behavior being dependent on the applied reverse bias, the operating temperature, the absorber thickness and doping, the series resistance and the electrical area of the devices. Fig. 12 shows the configuration of these devices.

HOT 5 μm cutoff MWIR imagers operating at 160 K were described with an emphasis on reduction in size, weight, and power. The 1024 \times 768 format camera utilizes 10 μm pixels and fits into a 6 \times 6 \times 5 cm package as shown in Fig. 13.

A first-principles derivation of an MWIR avalanche photodiode operation was described. Fig. 14 shows the calculated gain as a function of bias.



Fig. 13 Ultra-compact MWIR imaging engine with overall volume of 180 cm^3 .

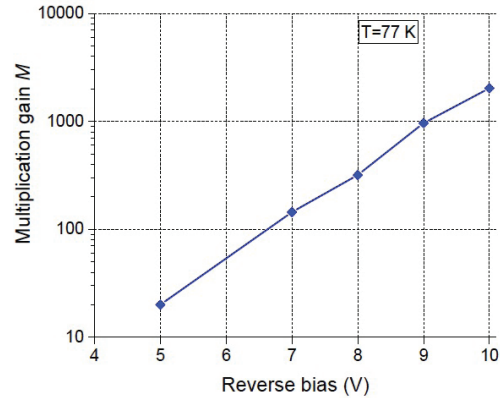


Fig. 14 Simulated gain as a function of reverse bias in MWIR HgCdTe at 77 K.

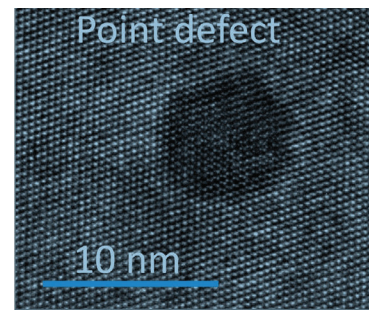


Fig. 15 Point defect in HgCdTe epilayer implanted by arsenic at 450keV after Hg overpressure annealing.

Arsenic ion-implantation into n-type HgCdTe is one method of diode formation in infrared detectors. Defects caused by this process were reviewed in a paper as a function of the implant energy and subsequent annealing. Fig. 15 show a point defect after 450 keV ion implantation and annealing that may be dominated by vacancies.

A wide-variety of techniques for constructing multi-spectral HgCdTe detectors was reviewed in another paper. These included back-to-back diodes, checker-board filters and plasmonic resonators.

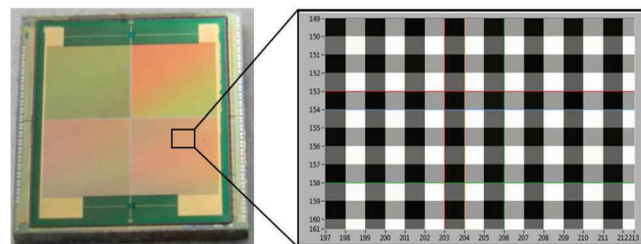


Fig. 16 15 μm pitch multicolor MWIR FPA after backside filter processing and raw image of a 4-color sub-array.

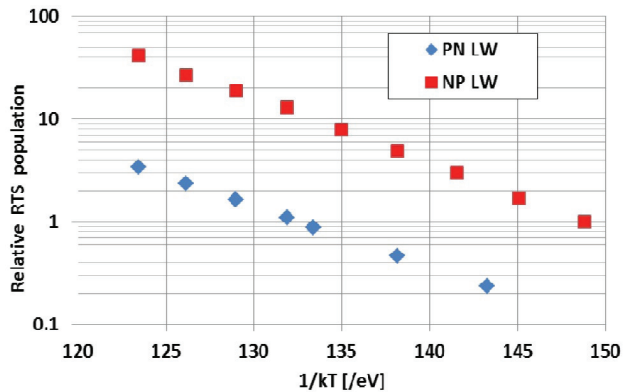


Fig. 17 Improvement in the relative population of random telegraph signal (RTS) noise in going from n-on-p polarity diodes to p-on-n polarity.

Several years of significant improvement in detector performance in going from *n-on-p* polarity diodes to *p-on-n* polarity was described in detail. A significant improvement was made in dark current, MTF, fixed pattern noise, and random telegraph signal noise—see Fig. 17. The dark current and quantum efficiency were also compared to results with Type II superlattice detectors.

Production scheduling strategies for complex infrared camera systems were discussed in a paper covering the introduction of small 10 μm pixel FPA formats.

The plasma etch rate of HgCdTe was studied at cryogenic temperature in addition to the smoothness of the sidewalls. Mask materials were also examined.

InSb

A 1280 \times 1024 InSb detector array development program was reported.

High Operating Temperature (HOT) FPAs

The goal of increasing the operating temperature of FPAs without sacrificing performance is motivated by the reduction in cooler power, improved cooler efficiency, longer cooler lifetime, smaller imager size, and lighter weight sensor systems that this makes possible. This goal is being pursued using HgCdTe, Type II superlattices, and *nBn* materials and has relevance especially in the MWIR and LWIR spectral bands.

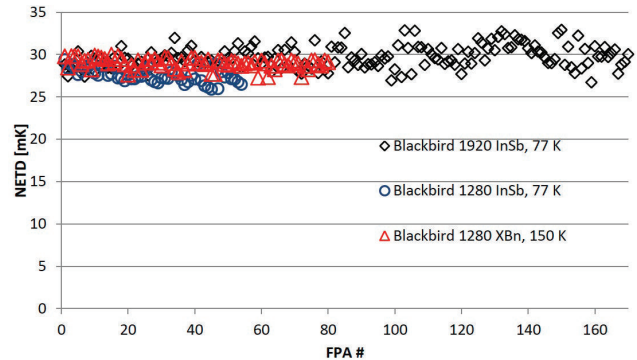


Fig. 18 Averaged NE ΔT values for InSb and XBn FPAs at 60 % well-fill from an MWIR production line. Note that the XBn detectors are operating at 150 K compared to 77 K for InSb.

InSb and *XBn* detector performance were compared in a paper on MWIR imaging. Uniform detectors have been made using both technologies and Fig. 18 shows that the NE ΔT for each are similar although the *XBn* can operate at about twice the temperature of InSb. The *XBn* devices cover only the blue-portion of the MWIR spectrum— $\leq 4.2 \mu\text{m}$ —and require a longer time to collect enough charge to fill the well to 60 %.

A high definition, 1156 \times 2040 FPA with 5 μm pixels was described. This device, operating at 150 K, has a cutoff of 5.1 μm with a dark current of $2.3 \times 10^{-5} \text{ A/cm}^2$ and 60 % quantum efficiency. Operability of 99.9 % demonstrates that 5 μm pixels can be fabricated in large arrays with excellent yield.

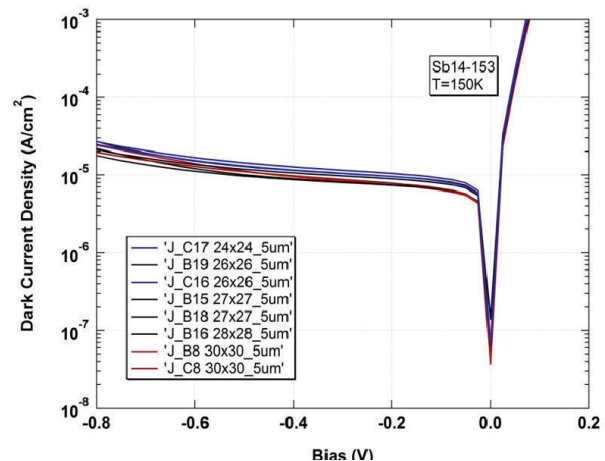


Fig. 19 Dark current I-V curves of 5 μm -pitch mini-arrays of various dimensions. Each detector array chip contains mini-arrays, which are quickly tested as representative predictors of FPA performance. The dark current density of $2 \times 10^{-5} \text{ A/cm}^2$ at the turn-on voltage of -150 mV compares favorably with similar devices at larger pixel pitches.

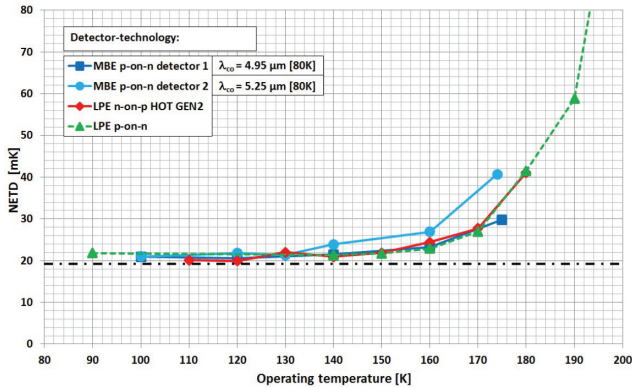


Fig. 20 Mean NEAT as a function of operating temperature for MWIR FPAs with MBE and LPE grown material. Note the diode polarity.

A large format HgCdTe detector array of 1024×768 pixels with a $10 \mu\text{m}$ pitch was reported with a $5.3 \mu\text{m}$ cutoff and an NEAT of 20 mK up to 150 K. Progress was reported in raising the operating temperature for a variety of HgCdTe material and diode types covering both MWIR and LWIR bands.

A paper was presented on *nBn* MWIR photodetectors based on bulk $\text{InAs}_{0.81}\text{Sb}_{0.19}$ with a $>5 \mu\text{m}$ cutoff operating at higher temperatures than InSb. Fig. 21 shows the dark current and components of the dark current from analysis of the bias dependence. At 150 K the quantum efficiency was 44 % at $3.4 \mu\text{m}$ and the D^* was reported to be 4.3×10^{11} Jones at $5 \mu\text{m}$.

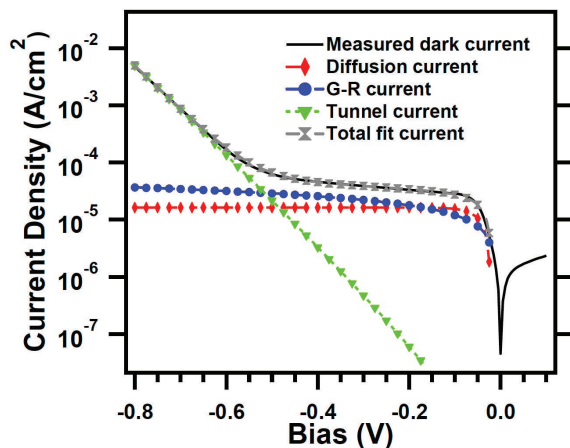


Fig. 21 Dark current density vs. bias measured at 150 K (black curve), total dark current fit (grey hourglass markers), along with diffusion (red diamond markers), G-R (blue circle markers), and tunneling (green triangle markers) components of the dark current fit.

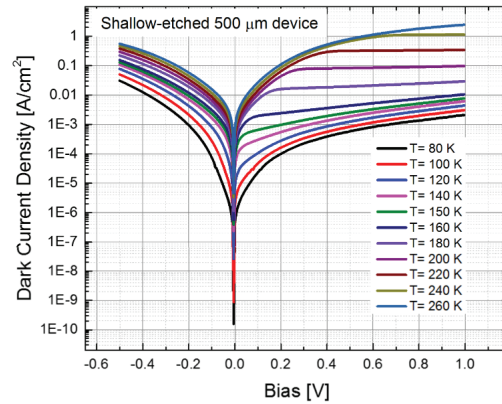


Fig. 22 The dark current density of the MWIR *nBp* photodetector as a function of bias voltage at various temperatures.

A high-quantum efficiency MWIR— $5 \mu\text{m}$ cutoff—superlattice detector in an *nBp* configuration was described having 64 % quantum efficiency at 150 K with a dark current density of $1.1 \times 10^{-4} \text{ A/cm}^2$. Fig. 22 shows the dark current density as a function of bias at a range of temperatures between 80 and 260 K.

A report on heterojunction bipolar phototransistor modeling presented design criteria aimed at realizing single-photon detection in the SWIR band. The device was fabricated with InP/InGaAs material as shown in Fig. 23. Sensitivity and gain issues related to these devices were discussed.

The superlattice materials can run into difficulties when carriers have difficulty propagating in the direction perpendicular to the alternating superlattice layers. Although the lifetime may be increased, carrier collection at the contacts can be compromised. This issue was discussed in a paper on carrier localization in which “digital” InSb layers were inserted into an InAsSb alloy *nBn* detector structure

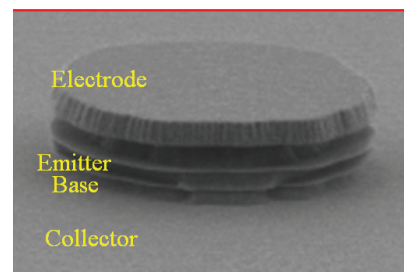


Fig. 23 SEM image of the fabricated heterojunction bipolar transistors with InP/InGaAs.

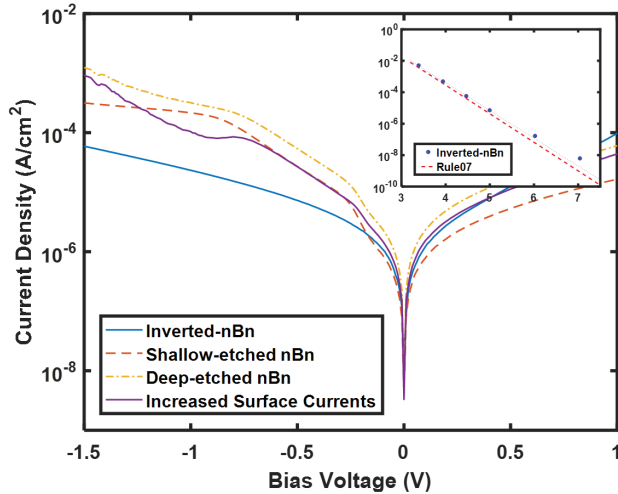


Fig. 24 I-V characteristics of the inverted-nBn, shallow-etched nBn and the deep-etched nBn at 200K. The inverted-nBn device has the lowest dark current. Its current density is much lower than the estimated increased surface currents that due to the barrier etching. Inset is the Arrhenius plot of the current density vs. $1000/T$ (K^{-1}) for the inverted-nBn device. A full bandgap thermal activation energy is seen in the measured temperature range.

A key advantage of *nBn* detector structures is the lack of a passivation problem by using the wide-bandgap barrier layer to provide that function. In conventional *nBn* devices, with the absorber on the bottom, lateral collection can limit the modulation transfer function. A paper was presented demonstrating how this problem can be overcome by inverting the structure. Fig. 24 shows the improvement in dark current density.

QWIP and colloidal quantum dot (CQD) detectors

Although a mature and aging technology, quantum well infrared photodetectors (QWIPs) are still evolving, especially to fill niche roles, such as a $10.6 \mu\text{m}$ laser detector. High-resolution and higher sensitivity advances in this technology were presented. An innovative flexible structure quantum well was developed, and could be physically deformed and even rolled up. This architecture allows increased photon absorption without gratings. The result is increased sensitivity over a broader band, potentially at a lower price.

Perhaps the most promising technology for low-cost, albeit, lower-sensitivity, focal planes are quantum dots. This technology has the promise of very low-cost, high-definition infrared FPAs from SWIR to VLWIR, at higher than typical temperatures. It is un-

likely that they will ever achieve the performance of InGaAs, HgCdTe, or InSb, and do require cooling; so they will likely be used in newer applications that require high definition low cost imaging on smaller pixels that doesn't require extreme sensitivity. Their fundamental properties appear to be potentially game changing as it is what infrared system engineers and customers desire. These properties include small pixel high performance, the lack of difficulty in HD arrays and the size of the ROICS that they are deposited on, and the super low cost, estimated at $< \$10$ per HD array. However, the requirement for cooling and ROIC cost will still make these more expensive than low resolution uncooled, but they may be less expensive than HD uncooled.

Initial characterization and understanding the transport and quantum efficiency barriers is key and papers were presented on such showing substantial progress. Fig. 25 illustrates the capture and transport mechanism of a colloidal dot film. One paper explored unipolar and bipolar QDot doping as well as structures with n-doping of layers, structures with n-doping of barriers, and structures with p-doping of quantum dot layers and n-doping of inter-dot space. Decent 320×240 images at 400 mK were shown using a process that is estimated to be less than $\$5$ per FPA using wet chemistry colloidal quantum dots deposited on a ROIC, with a dropper. Figure 26 is an example of an image from a quantum dot FPA.

There seems to be a nomenclature issue in our community, some authors calling this technology: QD (quantum dots), QDots (for quantum dots), QDIPs (Quantum Dot Infrared Photodetectors) and other using a more specific CQD (Colloidal Quantum Dots). Presently, for this embryonic detection technology, we suggest that authors use several acronyms: QD for

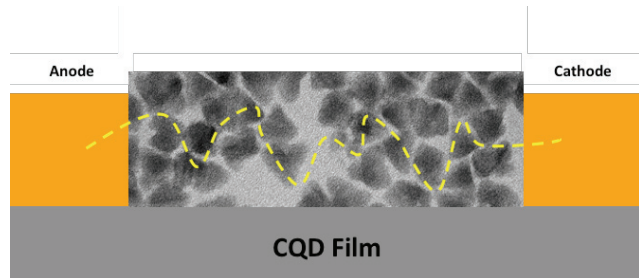


Fig. 25 An SEM Image of a PV quantum dot detector and how the authors imagine that a photo-generated charge is transported.



Fig. 26 An infrared image acquired by a quantum dot FPA.

any type of quantum dot—epitaxial or colloidal, CQD for colloidal quantum dot, and QDIP for PC or PV detectors based on QD absorbers. However, we hope in the future for a more accurate and encompassing nomenclature.

Uncooled Detectors

There continues to be significant interest in novel absorbers for customizing the spectral and polarization discrimination in low-cost sensors. Reports of progress regarding plasmonic absorption show promise for hyperspectral imaging at the lower end of the performance range. On the other hand, a novel implementation of gold-black coatings in conjunction with a compatible packaging technology offers the possibility of extremely broadband sensing with minimal compromise of response time.

A related topic of recent interest is the use of low-dimensional materials such as graphene and NanoWires (NWs) for infrared detection, including the use of hybrid structures and heterostructures. These proposed devices are somewhat speculative, and generally count on plasmonic structures for adequate infrared absorption. Some of the proposed structures are illustrated conceptually in Fig. 27.

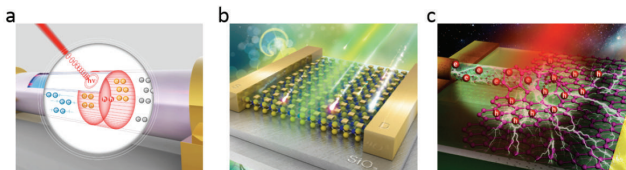


Fig. 27 (a) schematic diagram of photogating induced negative photoconductivity for infrared single InAs NW photodetectors; (b) schematic view of surface plasmon enhanced 2D photodetectors; (c) schematic view of heterojunction based on 1D NWs and 2D materials.

There has been substantial progress toward implementation of a fully-CMOS bolometer technology that may provide an alternative to thermopiles as a solution for smart-building applications. This technology offers hope for superior performance at competitive prices.

The uncooled session continues to be marked by the absence of papers from the high-volume producers of FPAs and sensors, because of the intense competition among numerous producers. However, the paper solicitation process this year indicated hopeful promise for revitalization of leading-edge papers next year, as some companies seem eager to boast of their unique near-term technical advantages relative to the competition.

ROICs

The Read out Integrated Circuit (ROIC) is increasing its role in system performance, by integrating advanced processing into the unit cell, rather than merely collecting the photo-generated charge. Evolutionary advances in ROICs continues, including advanced integrated analog to digital conversion, programmability and on-chip corrections. A paper was presented about a $0.18\ \mu\text{m}$ process ROIC, with 13-million electron well capacity with programmable features. Additionally, ROICs are being developed for full HD and even larger formats.

Smart Processing

In addition to advanced processing on the ROIC, new techniques for infrared imaging and off chip processing also promises great system level advances. In the “Smart Processing” Session there was a paper on a 2.4 megapixel MWIR FPA with large scale over-sampling of the blur spot. The author claimed that 9-to-25 pixels in an optical blur produces optimal imaging in most situations. There was some disagreement on the amount of over-sampling that is optimum, many suggesting a smaller amount.

The paper states that challenges in sub-wavelength pixel FPAs include “pixel transimpedance gains that allow near BLIP operation over expected back-



Fig. 28 Local suspect shown in an MWIR image from a 2040×1156 FPA having $5 \mu\text{m}$ pixels.

grounds, the development of low leakage detectors with low lateral diffusion lengths, and high yield detector-to-ROIC integration techniques. The long term vision of spatial over-sampling is that of smaller sub-diffraction size pixel FPAs with larger formats. The smaller pixels will enable shorter focal lengths for a given instantaneous field of view (IFOV), allowing more compact sensors with smaller optics.” An example of a 2.4-megapixel over-sampled image is presented illustrated in Fig. 28.

Applications

Presentations focusing on applications of the various infrared technologies in systems and subsystems were presented in Oral Session 3 and in the Posters session. As is usual in our Proceedings, the Poster papers will appear in their appropriate sections for Oral papers. Applications, being the main drivers for technology R&D, are also referred to in the more technology-focused papers throughout the Proceedings.

The invited session on IR in Air and Space focused almost entirely on spectral and hyper-spectral instrumentation. Two national institutes reviewed their space-borne imaging systems for atmospheric studies. One discussed the use of a curved prism for improving the optical efficiency over the NIR and SWIR spectral bands—see Fig. 29. A Ground Motion Compensation technology was incorporated in order to increase SNR obtained from the Tiangong spacecraft’s hyper-spectral imager.

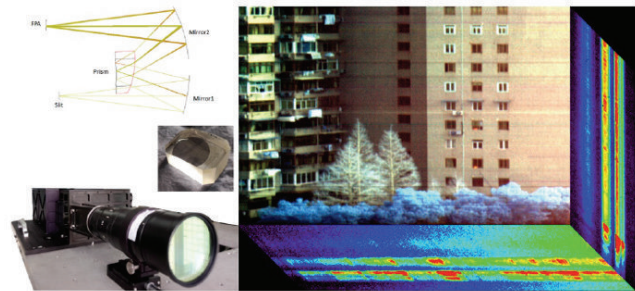


Fig. 29 NEAT for a $9 \mu\text{m}$ cutoff array with $12 \mu\text{m}$ pixels in a 1280×720 format.

The other institute presented their MWIR CubeSat Infrared Atmospheric Sounder (CIRAS) which employs an immersion grating spectrometer with no moving parts. The CIRAS instrument outlined in Fig. 30 includes a scan mirror capable of rotating 360° to view Earth, cold space and an internal blackbody for calibration. The optics, detectors and blackbody were discussed in some detail.

While CIRAS’ MWIR spectrometer employs a photon detector based on GaInAsSb/GaAlSbAs semiconductor material and operating at 120 K temperature, a geophysics institute considers making hyper-spectral imaging MWIR measurements from space with an instrument based on an uncooled detector. With recent improvements in microbolometer technology and interferometric techniques, they have investigated the performance of their low mass and low power consumption MIDAS instrument against relatively high

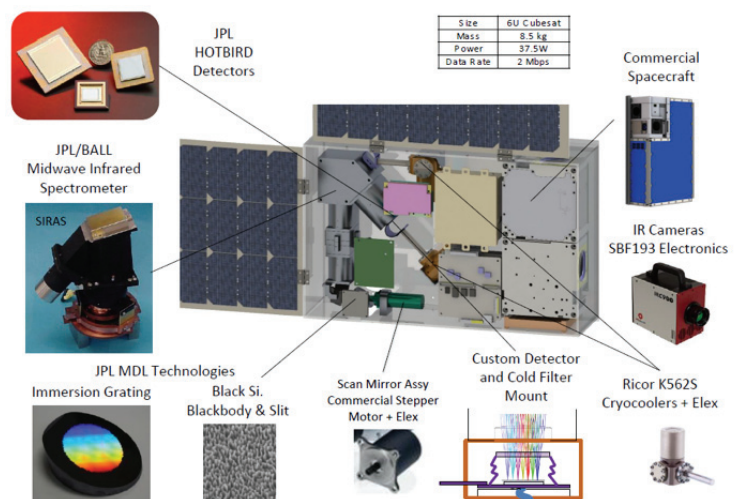


Fig. 30 The CIRAS infrared atmospheric sounder.

temperature phenomena such as wildfires and active lavas.

A sensor's small size and weight are the main design drivers also for a hyper-spectral imager payload mounted on a miniature unmanned aerial vehicle or on a commercial quadcopter. One company presented a new and innovative approach using diffractive micro-optical elements for their infrared hyperspectral imaging spectrometer—see Fig. 31. An application of the sensor for quantifying the flow rate of a gas was demonstrated.

The three remaining application presentations were all ground-oriented. One company presented the considerations involved in replacing classic episcopes/periscopes with cameras and monitors for use as situational awareness systems in battle tanks. Their TIV system is based on the Distributed Aperture System (DAS) principle and results in great weight and volume reduction inside the tank turret.

A university group proposed a novel method for detection of pedestrians at ranges above 50 meters. Data obtained from a LWIR camera was used to define regions of interest (ROI). The detection probability was then increased by classifying the ROIs using transfer learning with a convolutional neural network (CNN) feature, followed by non-maximal suppression (NMS) with strong aspect ratio limitation. Experimental validation tests were described in some detail.

Another academic group has analyzed several landmine detection algorithms as well as their fusion. Their relative performance was determined using sig-

nals obtained from an infrared imager. The measurements were made on mines buried at various depths in a sandbox. Effects of changes in the environment, soil and type of land mine were investigated. The most robust algorithm was identified.

A Word from the Masters

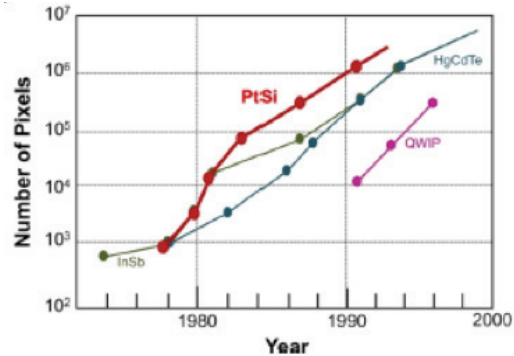


Fig. 32 PtSi ten-year pixel-count dominance

Professor Masafumi Kimata of Ritsumeikan University in Japan gave a review of his near forty-years of R&D in the infrared field. The first part of this long and fruitful time was spent in industry where one of his many accomplishments was the development of the World's-first megapixel IRFPA. Fig. 32 shows the PtSi Schottky-diode ten year pixel-count dominance. He also was instrumental in developing the uncooled SOI FPA—see Fig. 33—which competes with the microbolometer due to better uniformity and lower noise. Japan's successful Infrared Array Sensor Forum (IRASF) was established and is being chaired by Professor Kimata.

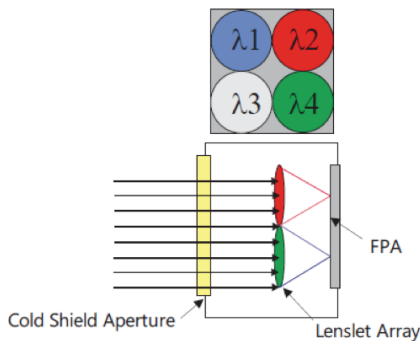


Fig. 31 Concept of a 2 × 2 lenslet array imaging on a focal plane array.

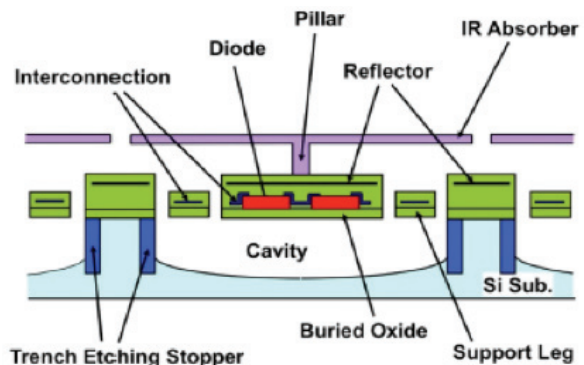


Fig. 33 Cross-sectional structure of SOI diode pixel

Ian Baker from Leonardo (formerly Selex) discussed his current interests in using state-of-the-art infrared sensors to address science advances in astronomy. A key component in this quest is the electron avalanche photodiode (eAPD). MOCVD material growth has made possible the fabrication of defect-free arrays—see Fig. 34—that are able to meet the requirements for challenging astronomy applications with avalanche gains as high as 500. This enabled adaptive-optic atmospheric correction using dim reference stars for the wavefront sensor in a campaign to image a star passing near a black hole. The technology is currently limited by readout glow. Fig. 35 shows the dark current as a function of bias voltage for a range of operating temperatures. The readout glow limit is shown for reference. Larger arrays and improved performance are in the works for future wavefront sensor missions on the 39 meter European telescope under construction in Chile.

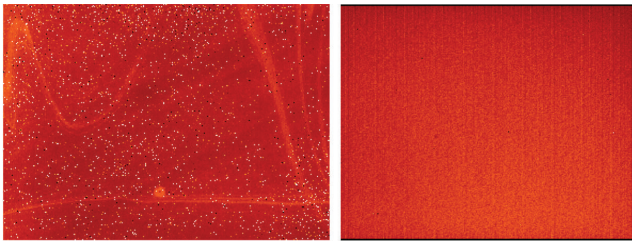


Fig. 34 Left: LPE e-APD array at 45K, operating with avalanche gain of 17. Right: MOVPE APD array at 85K, operating with avalanche gain of 59.

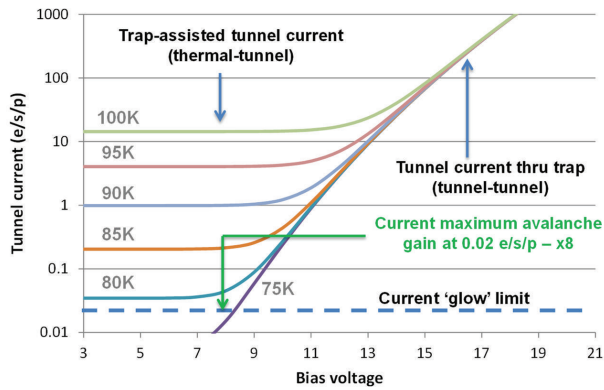


Fig. 35 Dark current of state-of-the-art HgCdTe e-APDs versus bias voltage showing an avalanche gain of 8 at the level of 0.02 e/s/p (electrons per second per pixel).

Keynote address

The keynote address reported on infrared detector development in support of China's weather satellite fleet. Fig. 36 shows an example of imagery from a second-generation earth-imaging instrument. Both HgCdTe and quantum well detector technologies are being pursued for this multi-faceted application. Advances in instruments for the next generation of these satellites were described, including an atmospheric sounder with 16 km spatial resolution for measuring temperature and humidity.

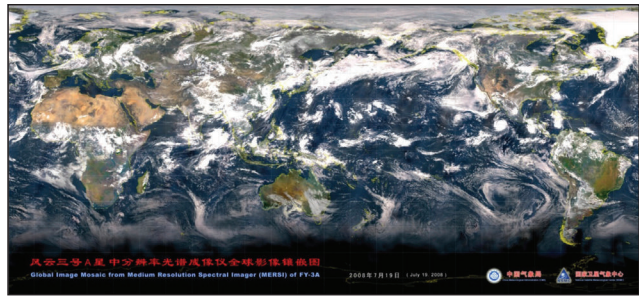


Fig. 36 The global image mosaic from the second-generation Medium-Resolution Spectral Imager (MERSI) of FY-3A observed in 19 July 2008.

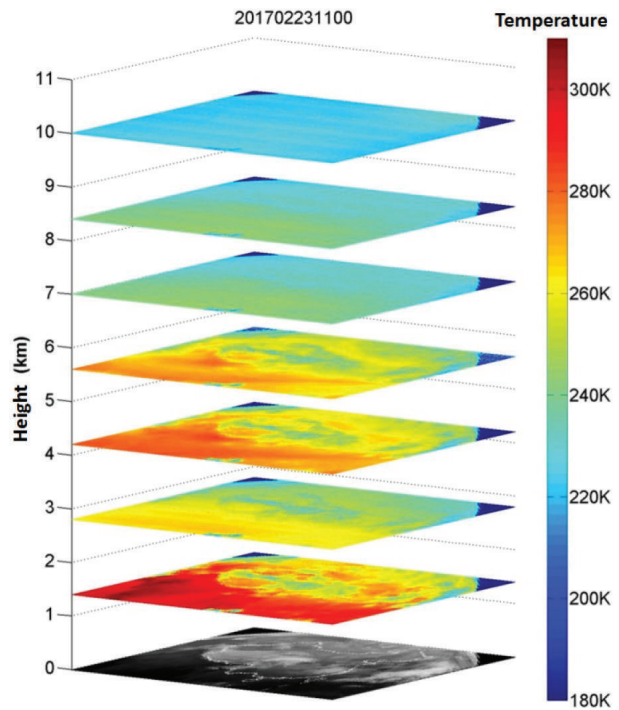


Fig. 37 The 3 dimensional temperature profile obtained by geostationary interferometric infrared sounder with 16 km spatial resolution on FY-4.

In remembrance

This year's Infrared Technology and Applications conference is dedicated to the memory of Joe Yaver—the maker of the modern SPIE—who passed away at the age of 83 last November. Our conference was the brainchild in 1975 of Irv Spiro, a scientist from the Aerospace Corporation in Los Angeles, and Joe Yaver, SPIE's Executive Director from November 1969 until 1993. Among his many accomplishments we would like to mention one—his launching of the “Technical Symposium Southeast” in Orlando. This Symposium was the precursor to our 2017 Symposium in Anaheim, the “Defense and Commercial Sensing” symposium.



Joe Yaver visiting SPIE Headquarter 2002



Paul R. Norton



Bjørn F. Andresen



Gabor F. Fulop



Charles M. Hanson



John Miller

